



# Numerical simulation of grassland fires behavior using an implicit physical multiphase model

Nicolas Frangieh, Dominique Morvan, Sofiane Meradji, Gilbert Accary, Oleg Bessonov

## ► To cite this version:

Nicolas Frangieh, Dominique Morvan, Sofiane Meradji, Gilbert Accary, Oleg Bessonov. Numerical simulation of grassland fires behavior using an implicit physical multiphase model. *Fire Safety Journal*, 2018, 102, pp.37-47. 10.1016/j.firesaf.2018.06.004 . hal-02114073

**HAL Id: hal-02114073**

**<https://amu.hal.science/hal-02114073>**

Submitted on 29 Apr 2019

**HAL** is a multi-disciplinary open access archive for the deposit and dissemination of scientific research documents, whether they are published or not. The documents may come from teaching and research institutions in France or abroad, or from public or private research centers.

L'archive ouverte pluridisciplinaire **HAL**, est destinée au dépôt et à la diffusion de documents scientifiques de niveau recherche, publiés ou non, émanant des établissements d'enseignement et de recherche français ou étrangers, des laboratoires publics ou privés.

# Accepted Manuscript

## Numerical Simulation of Grassland Fires Behavior Using an Implicit Physical Multiphase Model

N. Frangieh, D. Morvan, S. Meradji, G. Accary, O. Bessonov



PII: S0379-7112(18)30037-7

DOI: 10.1016/j.firesaf.2018.06.004

Reference: FISJ 2718

To appear in: *Fire Safety Journal*

Received Date: 29 January 2018

Accepted Date: 18 June 2018

Please cite this article as: N. Frangieh, D. Morvan, S. Meradji, G. Accary, O. Bessonov, Numerical Simulation of Grassland Fires Behavior Using an Implicit Physical Multiphase Model, *Fire Safety Journal* (2018), doi: 10.1016/j.firesaf.2018.06.004

This is a PDF file of an unedited manuscript that has been accepted for publication. As a service to our customers we are providing this early version of the manuscript. The manuscript will undergo copyediting, typesetting, and review of the resulting proof before it is published in its final form. Please note that during the production process errors may be discovered which could affect the content, and all legal disclaimers that apply to the journal pertain.

# Numerical Simulation of Grassland Fires Behavior Using an Implicit Physical Multiphase Model

N. Frangieh<sup>1</sup>, D. Morvan<sup>1,\*</sup>, S. Meradji<sup>2</sup>, G. Accary<sup>3</sup>, O. Bessonov<sup>4</sup>

<sup>1</sup> Aix-Marseille Université, CNRS, Centrale Marseille, M2P2, Marseille, France

<sup>2</sup> IMATH laboratory, EA 2134, Toulon University, France

<sup>3</sup> Scientific Research Center in Engineering, Lebanese University, Lebanon

<sup>5</sup> Institute for Problems in Mechanics, Russian Academy of Sciences, Russia

(\*) Corresponding author (dominique.morvan@uni-amu.fr)

## Abstract

This study reports 3D numerical simulations of the ignition and the propagation of grassland fires. The mathematical model is based on a multiphase formulation and on a homogenization approach that consists in averaging the conservation equations (mass, momentum, energy ...) governing the evolution of variables representing the state of the vegetation/atmosphere system, inside a control volume containing both the solid-vegetation phase and the surrounding gaseous phase. This preliminary operation results in the introduction of source/sink additional terms representing the interaction between the gaseous phase and the solid-fuel particles. This study was conducted at large scale in grassland because it represents the scale at which the behavior of the fire front presents most similarities with full scale wildfires and also because of the existence of a large number of relatively well controlled experiments performed in Australia and in the United States. The simulations were performed for a tall grass, on a flat terrain, and for six values of the 10-m open wind speed ranged between 1 and 12 m/s. The results are in fairly good agreement with experimental data, with the predictions of operational empirical and semi-empirical models, such as the McArthur model (MK5) in Australia and the Rothel model (BEHAVE) in USA, as well as with the predictions of other fully 3D physical fire models (FIRETEC and WFDS). The comparison with the literature was mainly based on the estimation of the rate of fire spread (ROS) and of the fire intensity, as well as on the analysis of the fire-front shape.

**Keywords:** Grassland fires, fire modeling, turbulent reactive flows, numerical simulation, high performance computing.

## 1. Introduction

Wildfire can be considered as a natural disaster or a necessary perturbation in the life of an ecosystem, depending on the place where this event occurs and on its intensity. The frontier between these two points of view depends strongly on the impact of this event on the environment and the economy, as well as on the management and the land use between natural and urban areas[1]. The ecologists often consider that the existence of low intense fires in natural areas (such as the national parks) is necessary to maintain locally the biodiversity, whereas many citizens can consider them as an unsupportable degradation of the environment, assimilated here as a recreation area. The fire regime, defined by integrating a set of characteristic parameters of fires (patterns, intensity, and frequency) for which an ecosystem presents an optimum resilience, is a good indicator of the level of perturbation caused by external factors such as climate changes or the level

of anthropization [2]. Various factors have in the past and can in the future, cause great modifications in the fire regime in a local area, such as the European settlement in America, in Australia, and in other parts of the world, the rural exodus, and global warming [3]. These changes can be particularly dramatic, when very intense fires occur in the wildland-urban interface (WUI) as it happened in Victoria state in Australia in 2009 (Black Saturday) [4] and more recently in 2016 in Alberta (Canada) near the city of Fort McMurray. To have an idea of the level of destruction of such “natural” hazard (a lot of fire ignitions have human caused), one of the fires occurring during the “Black Saturday” event (the Kilmore East fire), had burnt more than 125 000 ha of forest, tree plantations and shrubs (100 000 ha in less than 12 hours), had caused 232 casualties (and 119 injuries), and had destroyed 1242 houses [4,5]. The fireline intensity was evaluated to 88 000 kW/m (in comparison, the average power of a unit in a nuclear power plant is about 1500 MW) [3].

Due to the extreme complexity of the problem, most of operational tools predicting wildfires behavior (such as PHOENIX [6] in Australia and FARSITE in USA [7]) are based on statistical or semi-empirical approaches, namely the MacArthur MK5 model [8,9] in Australia and the Rothermel model (BEHAVE) in USA [10]. However, in many situations, especially that deviate from the conditions on which these models were calibrated, the quality of the predictions compared to real observations collected on well documented fire can be qualified as poor [11]. These tools propose to evaluate some characteristic parameters of fire, such as the rate of spread (ROS), the fire intensity, and the flame height. However, the validity of the predictions of empirical models are limited to the range of parameters used to develop the statistical laws. As for semi-empirical models, such as BEHAVE, predictions at large scale are of poor quality because most of them are made by extrapolation of data obtained from small-scale fires performed in a wind tunnel through homogeneous dead fuel bed (pine needles, excelsior, sticks) [11], which may lead sometimes to unexpected results such as a ROS greater than the wind speed. Such behavior cannot be explained physically, except in the case of no wind fires or in the absence of propagation mechanisms other than heat transfer by convection and radiation between the flame front and the vegetation (by spot particles for example), because the sum of characteristic times associated with the physical process necessary for the propagation of the fire (drying, pyrolysis, combustion ...) is larger than the travel time characterizing the wind flow. Consequently, other approaches have been proposed to improve the knowledge of the physical process responsible of the fire behavior. These alternative class of fire models are based on more or less realistic description of the physical phenomena governing the heat transfer between the fire front and the vegetation [12]. A fully physical model addresses the problem of fire spread by analyzing its behavior through its physicochemical aspects [13,14]. This approach minimizes the need of using an empirical parameterization, even if, compared to empirical and semi-empirical models, it needs bigger computational resources (which limit their capability in solving the problem in real time), it is also more promising in the understanding of the physics of fires [11, 15–18]. The fully physical approach has also a great potential in the management of fire hazard in wildland urban interfaces, using an engineering approach, such as the dimensioning of a fuel break, the evaluation of heat flux on a target located inside the WUI, the interaction between two fire fronts [19–22].

The 3D model described in this work is based on a multiphase formulation and solves the conservation equations of the coupled system formed by the vegetation and the surrounding gaseous medium [13,18,23]. The model takes into account the vegetation

degradation processes (drying, pyrolysis, and combustion), the interaction between the atmospheric boundary layer and vegetation (aerodynamic drag, heat transfer by convection and radiation, and mass transfer), and the transport in the gaseous phase (convection, turbulence, and combustion). The model is implemented in a modular and parallelized 3D computation code referred to as "FireStar3D". The code is based on a finite volume discretization of the governing transport equations (3<sup>rd</sup> order in time and 2<sup>nd</sup> order in space) and has undergone numerous validations [23–26]. The predictive potential of FireStar3D model was tested at a small scale in the case of litter fires (fire propagation through a homogeneous fuelbed in a wind tunnel) [23]. The objective of this study is to extend the tests at a larger scale for grassland fires. Grassfires have the great advantage to have been extensively studied experimentally, in very good conditions, especially the experimental campaigns carried out in Australia [27–29], which are considered as a good benchmark to test wildfire physical models [15,16,30]. For different wind speeds, fire behavior and spread through homogeneous grassland is analyzed in terms of rate of fire spread, fire intensity, and shape of the fire front. The results were compared with data collected during experimental campaigns and predictions from semi-empirical and other physical models.

## 2. Modeling and Numerical Method

The mathematical model is based on a multiphase formulation, it consists in a first step of averaging the conservation equations (mass, momentum, energy ...) governing the behavior of the coupled system formed by the vegetation and the surrounding atmosphere inside elementary control volumes including both the solid phase (the vegetation) and the gaseous phase. This first operation, similar to a homogenization step, results in the introduction of source/sink terms on the right hand side of the equations, representing the contributions of the interaction terms (exchanges of mass, drag, heat flux ...) between the gaseous phase and the vegetation. The details of the model have been widely presented in previous publications, we invite the reader to consult references [13,14,17,18,30] for more information.

The model consists of two parts that are solved on two distinct grids. The first part consists of the equations of a reacting turbulent flow in the gaseous phase composed as a mixture of fresh air with the gaseous products resulting from the degradation of the solid phase (by drying, pyrolysis, and heterogeneous combustion) and the homogeneous combustion in the flaming zone. The second part consists of the equations governing the state and the composition of the solid phase subjected to an intense heat flux coming from the flaming zone.

Solving the gaseous phase model consists in the resolution of conservation equations of mass, momentum, energy (in enthalpy formulation), and chemical species ( $O_2$ ,  $N_2$ ,  $CO$ ,  $CO_2$ , and  $H_2O$ ) filtered using an unsteady RANS approach (TRANS) with Favre average formulation [31]. The closure of the averaged conservation equations are based on the concept of eddy viscosity [32] obtained from an evaluation of the turbulent kinetic energy  $k$  and its dissipation rate  $\varepsilon$ . A high Reynolds number version of a two-equation statistical turbulence model ( $k$ - $\varepsilon$ ) is used with the RNG formalism [33,34]. The temperature dependence of the gas-mixture enthalpy is based on CHEMKIN thermodynamic tables [35]. A combustion model based on Eddy Dissipation Concept (EDC) [32,36] is used to evaluate the combustion rate occurring in the gaseous phase. Finally, because radiation heat transfer (mainly due to the presence of soot particles in the flame) plays an important role for the propagation of the fire front, the field of soot volume-fraction in

the gas mixture is calculated by solving a transport equation [37,38] including a thermophoretic contribution in the convective term and taking into consideration soot oxidation [39].

Concerning the solid phase model, during the thermal degradation, the composition of the solid fuel particles representing the vegetation is represented as a mixture of dry material (generic term for a mixing of cellulose, hemicellulose, and lignin), charcoal, moisture, and residual ashes. For each solid particle, the model consists in solving the equations governing the time evolutions of the mass fractions of water, of dry material, of charcoal, as well as of the total mass of the solid particle, its volume fraction and its temperature (the model does not assume a thermodynamics equilibrium between the gas mixture and solid fuel particles). The degradation of the vegetation is governed by three temperature-dependent mechanisms: drying, pyrolysis, and charcoal combustion. The pyrolysis process starts once the drying process is completed and charcoal combustion starts once the pyrolysis process is achieved. The constants of the model associated with the charcoal combustion (activation energy and pre-exponential factor) are evaluated empirically from a thermal analysis conducted on various solid fuels samples [13,40].

The interaction between the gaseous phase and the solid one is taken into account through coupling terms that appear in both parts of the model. The coupling in the momentum and turbulence equations is obtained by adding aerodynamic drag terms. These terms (both source and sink) are proportional to  $V$  (for turbulence destruction), to  $V^2$  (for the momentum equation), and to  $V^3$  (for turbulence production), where  $V$  is the local average of the velocity magnitude [30], and include a drag coefficient (evaluated empirically) multiplied by a reference surface, defined here as the Leaf Area Density (LAD). Heat transfer between the gas mixture and the solid fuel is based on empirical correlations for convective transfer coefficient [40], and on the resolution of the radiative transfer equation [41] that accounts for the presence of soot in the flaming zone and for the presence of hot particles in the vegetation layer (embers) [13]. Finally, mass transfer from the solid phase to the gaseous phase is represented by adding source/sink terms in the mass conservation equations of both phases.

The balance equations in the gaseous phase are solved numerically using a fully implicit finite volume method in a segregated formulation [42]. "FireStar3D" model predicts turbulent reacting flows in rectangular domains using a structured but non-uniform staggered mesh. Time discretization relies on a third order Euler scheme with variable time stepping strategy. To ensure numerical stability, space discretization is based on second order schemes with flux limiters (QUICK scheme [43,44]) for convective terms while diffusion terms are approached by central difference approximation with deferred corrections [45] to maintain the second order accuracy in space. The Radiative Transport Equation (RTE) is solved using a Discrete Ordinate Method (DOM), consisting in solving the radiation-intensity equation in a finite number of directions [46]. The radiative transfer equation accounts for gas-soot mixture absorption of radiative intensity depending on the amounts of combustion products ( $\text{CO}_2$  and  $\text{H}_2\text{O}$ ), on the gas mixture temperature, and of the soot volume fraction [47]. This set of discrete contributions is then integrated using a numerical Gaussian quadrature rule (a S8 method is used) for the calculation of the total irradiance. The set of ordinary differential equations describing the time evolution of solid-fuel state (mass, temperature, and composition) are solved separately using a fourth order Runge-Kutta method. From implementation point of view, the computation code is parallelized [48] and optimized [49] using OpenMP directives (operational on shared memory platforms and on Intel Xeon Phi coprocessors). Finally,

the hydrodynamic module of the code has been extensively validated on several benchmarks of laminar and turbulent natural convection, forced convection, and neutrally stratified flow within and above a sparse forest canopy [48–50].

Compared to the two main physical wildfire models referenced in the literature, i.e. WFDS [15] and FIRETEC [16], FireStar3D shares many similitudes with WFDS but it also presents important differences. In FireStar3D, as in WFDS, the flow solver is based on a low Mach number formulation, a real calculation of the turbulent combustion in the flame (using Eddy Dissipation Concept model), which is not the case in FIRETEC [30]. From a numerical point of view, FireStar3D is fully implicit whereas the solver in WFDS is explicit. One of the main differences at the modeling level with WFDS is related to the estimation of the radiation heat transfer from the flame. In WFDS, the radiative heat transfer is calculated but a minimum threshold value is fixed as a minimum radiative ratio from the energy released from homogeneous combustion; this arbitrary approach was not introduced in FireStar3D. These two characteristics, constitutes an important progress toward a more physical wildfire model, it represents also a great challenge in terms of computational resources.

### 3. Grassland Fire Configuration

As mentioned in introduction, the aim of this work is to show that the model is able to predict numerically the spread of a fire through grassland. A perspective view of the domain is shown in Fig. 1; the computational domain was 120 m long, 140 m wide, and 40 m high. The homogeneous vegetation layer, of height  $\delta = 0.7$  m, is 100 m long and 100 m wide, and it is located at 20 m from the domain inlet and at 20 m from the domain lateral boundaries. The main physical characteristics of the vegetation layer are given in Tab. 1. The heat yield of the fuel is 18000 kJ/kg, the solid fuel particles are assumed to behave as a black body, and a vegetation family of cylindrical shape was considered. The shape of the fuel particles is used for the description of their regression law and for the estimation of the heat transfer coefficient. For the solid phase, a uniform grid with  $(\Delta x, \Delta y, \Delta z) = (0.25 \text{ m}, 0.25 \text{ m}, 0.035 \text{ m})$  was used matching the vegetation zone, while a non-uniform grid of  $224 \times 248 \times 90$  cells was used for the fluid phase covering the whole computational domain. Within the vegetation zone, the fluid-phase grid was uniform with  $(\Delta x, \Delta y, \Delta z) = (0.5 \text{ m}, 0.5 \text{ m}, 0.07 \text{ m})$  and then it was coarsened gradually toward the open boundaries according to a geometric progression with common ratio 1.05. Both the solid-phase and the fluid-phase grids were characterized by cells sizes below the extinction length scale [14] within the vegetation given by  $4/\alpha\sigma$  and equal to 0.5 m in our case. This value should not be exceeded in order to avoid fire extinction especially in the case radiation-dominated fire propagation (i.e. when the wind speed is low to moderate). Furthermore, in the context of using a high Reynolds number turbulence model, the choice of the mesh size at the vicinity of solid bottom wall is strongly related to the quality of the obtained solution. The dimensionless distance to the wall  $z^+$  is defined by Eq. 1 where  $C_\mu = 0.0845$ ,  $k$  is the turbulent kinetic energy, and  $\rho$  and  $\mu$  respectively the density and the dynamic viscosity of gas mixture. The center of any cell adjacent to the bottom wall must have a dimensionless distance to the wall that satisfies the constraint  $11.5 < z^+ < 500$  [44] (i.e. the cell center lies within the fully turbulent zone), and this during the entire simulation time.

$$z^+ = \frac{\rho C_\mu^{1/4} k^{1/2} z}{\mu} \quad (1)$$

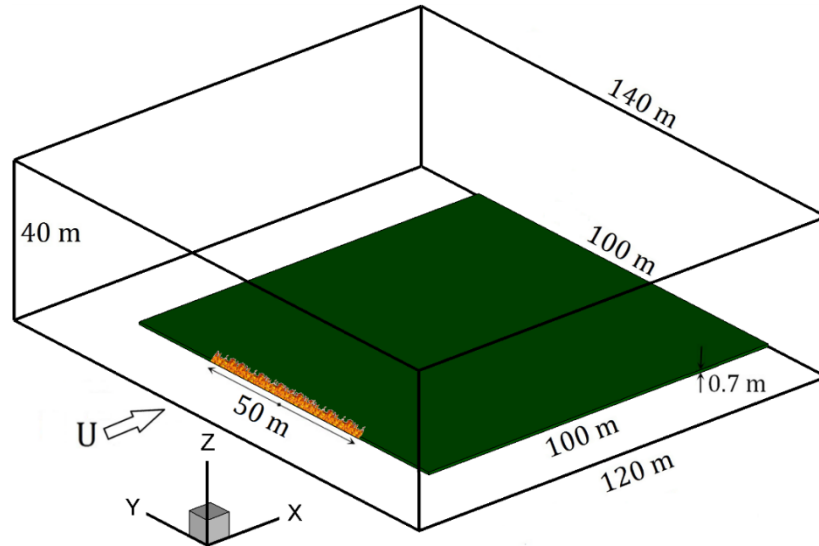


**Figure 1.** Perspective view showing the dimensions of the computational domain and of the vegetation cover. The ignition line is 2 m wide and 50 m long. In the non-uniform ignition mode, the burner is activated from the middle of the ignition line toward its ends at the speed of 1 m/s.

Burner activation occurs at time  $t = 10$  s, time for which the flow had reached a statistically-steady state, this phase was considered for the entire cases studied in this paper. During this (purely dynamic) flow settlement phase, homogeneous Neumann boundary conditions were imposed at the open boundaries of the computational domain for all primary variables of the problem excepted for  $y$  and  $z$ -velocity components where Dirichlet conditions (value set to zero) were imposed. In addition, a negative pressure gradient is applied in the wind direction ( $Ox$ ); this pressure gradient was automatically adjusted during the flow settlement phase to obtain the desired level of the 10-m open wind speed. This procedure allowed collecting the turbulent fields at the open boundaries, and these fields were then used during the burning phase, in particular for the management of the entering turbulent fluxes.

Vegetation height $\delta$ (m)	Solid-fuel volume-fraction $\alpha$	Surface/Volume ratio $\sigma$ ( $m^{-1}$ )	Dry material density $\rho$ ( $kg/m^3$ )	Moisture content $M$ (%)	Heat yield (kJ/kg)	Thermal emissivity	Vegetation family shape
0.7	0.002	4000	500	5	18000	1	Cylindrical

**Table 1.** Geometric and physical properties of the grassland vegetation [16,30]

At time  $t = 10$  s, the burner was activated along an ignition line, extends over  $w = 50$  m of length and 2 m of wide, as shown in Fig. 1. Fire was set by injecting CO gas at 1600 K in the burning zone from the bottom boundary of the domain. At time  $t = 10$  s, the average velocity  $V_{inj}$  of CO was maximum (equal to 0.1 m/s), and then it was decreased linearly with the consumed mass of solid-fuel according to equation (2). This procedure avoided destabilizing the flame front by abruptly ceasing the CO injection and avoided any excessive external energy input.



$$V_{inj} = \left(1 - \frac{m_b}{m_{b0}}\right) \times (0.1 \text{ m/s}) \quad (2)$$

In Eq. 2,  $m_{b0}$  represented the mass of dry material initially available above the burner area (i.e. the mass of dry material contained in the volume  $V_{b0} = 2 \times 50 \times \delta \text{ m}^3$ ). Equation 2 was used between  $t = 10 \text{ s}$  and  $t = 35 \text{ s}$  (i.e. during 25 s) as long as  $V_{inj}$  remained positive and CO injection ceased if  $V_{inj}$  reached zero during this time interval.

The parametric study focused on the influence of 10-m open wind speed on the fire behavior in terms of rate of spread, of fire intensity, and of shape of the fire front. The simulations were carried out for six values of the 10-m open wind speed: 1, 3, 5, 8, 10, and 12 m/s. These velocities were measured at the domain inlet, 10 m above ground. Two modes of fire ignition were considered: uniform and non-uniform, for the entire range of the wind speed  $U$ . In the uniform ignition mode, the burner was activated at the same time throughout the ignition zone. In the case of non-uniform ignition, the burner was activated from the middle of the ignition line (at  $y = 70 \text{ m}$ ) toward its two end sides (at  $y = 70 \pm 25 \text{ m}$ ) at the speed of 1 m/s.

The results presented in this study were obtained using a variable time step strategy based on the truncation-error control, with time step values varying between 0.001 s and 0.01 s. At each time step, the solution is assumed to be obtained when the residuals of all conservation equations had reached  $10^{-4}$  in normalized form. As a rough estimation of the computational cost, the simulation of 1s of fire propagation required about 7h of CPU time on a 28-cores node.

#### 4. Numerical Results

This numerical study focuses on fire spread through a grassland whose vegetation structure is quite homogeneous (see Fig. 2) and identical to a natural undisturbed grassland. The simulations were carried out under conditions similar to those of the Australian experimental campaign of 1986 [27–29]. The chosen configuration is very similar to experiment C064 of controlled fire conducted by Cheney et al. (1986) on a parcel of carefully cut grass [28] and shown in Fig. 3. However, the simulations were carried out for tall grass ( $\delta = 0.7 \text{ m}$ ) unlike experiment C064 ( $\delta = 0.21 \text{ m}$ ); this choice was mainly motivated by the existence of prior numerical studies [16,30]. In order to assess the predictive potential of the model, the results were compared to the predictions of the Australian empirical model MK5 [51], of the US semi-empirical model BEHAVE [52], of three-dimensional physical models (FIRETEC from LANL and WFDS from NIST), and of a two-dimensional physical model (FireStar2D [30]) that solved the problem of fire spread in a vertical plane perpendicular to an infinite ignition line.



**Figure 2.** Structure of the grassland vegetation (tall-grass) (from [https://commons.wikimedia.org/wiki/File:Dry\\_Grass.JPG](https://commons.wikimedia.org/wiki/File:Dry_Grass.JPG))



**Figure 3.** Photos of experiment 'C064 - AU Grassland Fire' carried out by Cheney et al. [28], 27s (left) and 53s (right) after fire ignition starts. Vegetation layer height  $\delta = 0.21\text{m}$ , fuel load  $\alpha\rho\delta = 0.28\text{ kg/m}^2$ , fuel surface/volume ratio  $\sigma = 9770\text{ m}^{-1}$ , moisture content  $M = 6.3\%$ , ignition-line length  $w = 50\text{ m}$ , wind speed  $U = 4.6\text{ m/s}$ .

#### 4.1. Fire Regimes and Fire-Front Shape

For a wind speed of  $5\text{ m/s}$ , Fig. 4 shows a top view of the propagation of a grassland fire uniformly ignited at time  $t = 10\text{ s}$  (in a  $2\text{ m}$ -wide and  $50\text{ m}$ -long strip). Time  $t = 35\text{ s}$  corresponds to end of ignition, unless the velocity of CO injection given by Eq. 1 had reached zero before that time. The pyrolysis front used to evaluate the ROS can be clearly seen on the mass fraction of the dry material. The results show: (i) the lateral fire spread in addition to the propagation in the wind direction, (ii) the ripple effect on the sides of the vegetation layer (visible at  $t = 55\text{ s}$  and  $t = 75\text{ s}$ ) when the pyrolysis front reaches these boundaries, and this effect becomes more visible with time (with more developed

ripples), (iii) the remote heating effect due to radiation, which is responsible for the drying of the fuel prior to arrival of the fire front, and (iv) the presence of some charcoal downstream the ignition line that continues burning behind the fire front due to the screening effect of CO injection that prevents the combustion of a part of charcoal downstream the ignition line. With time, we notice that the fire front loses gradually its parabolic shape and its forward-propagation speed becomes more important at the lateral sides than at the central part of the fire front. However, the leading point of the fire front remains nevertheless at the central part during the entire simulation. This effect is not only inherent to the ignition method but also to the ratio between the length of the ignition line and the lateral extent of the vegetation cover. Decreasing significantly this ratio should reduce this effect or might suppress it completely. Figure 5 is the counterpart of Fig. 4 using the non-uniform ignition mode. The idea is to represent the ignition method of experience C064, and more generally that of the Australian experimental campaign, where fire is set by two persons using a torch starting at the middle of the ignition line and walking in opposite direction at the speed of 1 m/s. Testing this ignition mode was motivated by the investigation of the parabolic shape of the fire front observed experimentally, as shown by Fig. 3 and as confirmed by other experiments, despite the observed loss of symmetry due to a change in the wind direction [28]. Other numerical simulations obtained using the same kind of fire physical model, have exhibited similar behavior, i.e. by igniting fire instantaneously along a sufficiently long width, the fire front keep a nearly linear shape (slightly incurved toward the back) in its central part [15]. A nearly parabolic front shape could only be reproduced numerically, if the ignition was restricted to a quite small line (less than 10m) or using a dynamical ignition procedure as in this study. Figure 5 shows in this case that the pyrolysis front is qualitatively more consistent with the experimental observations. It seems however that the ROS value (evaluated from the trajectory of the heading fire) is not significantly affected by the ignition method. This was certainly due to the fact that the initial width of the ignition line (50 m) was sufficiently long to not affect much the magnitude of the rate of spread. Experimental investigations have shown that above an ignition line equal to 50 m the rate of spread of the head fire was nearly equal to the theoretical value observed for an infinitively long fire front [28]. We can notice on both simulations, that the lateral expansion of the fire front (flank fire) was correctly reproduced, this is a good indicator of the quality of the model part in charge of the radiation heat transfer between the flame and the vegetation. This behavior was also correctly reproduced by simulations performed using WFDS, whereas it was underlined as one of the major point to improve in FIRETEC [16,53]. Figure 6 shows vertical profiles of primary variables at a duly chosen location corresponding approximately to the furthestmost point of the fire front in Fig. 5 (at  $t = 35$  s). The figure highlights the appropriate mesh resolution for the evaluation of the resolved-variables gradients and the production of the turbulent kinetic energy at the surface of the fuel bed. To illustrate the remote heating effect mentioned earlier, figure 7 shows that the solid-fuel temperature at the fuel-bed surface exceeds that of the gas mixture ahead of the fire front (located from the mass fraction of dry material). This means that the increase of the solid-fuel temperature is not the result convection heat transfer from the gas mixture. Consequently and as mentioned before, this remote heating can only be imputed to radiative heat transfer from the flaming zone, resulting in the water content loss observed ahead of the fire front in Fig. 7.

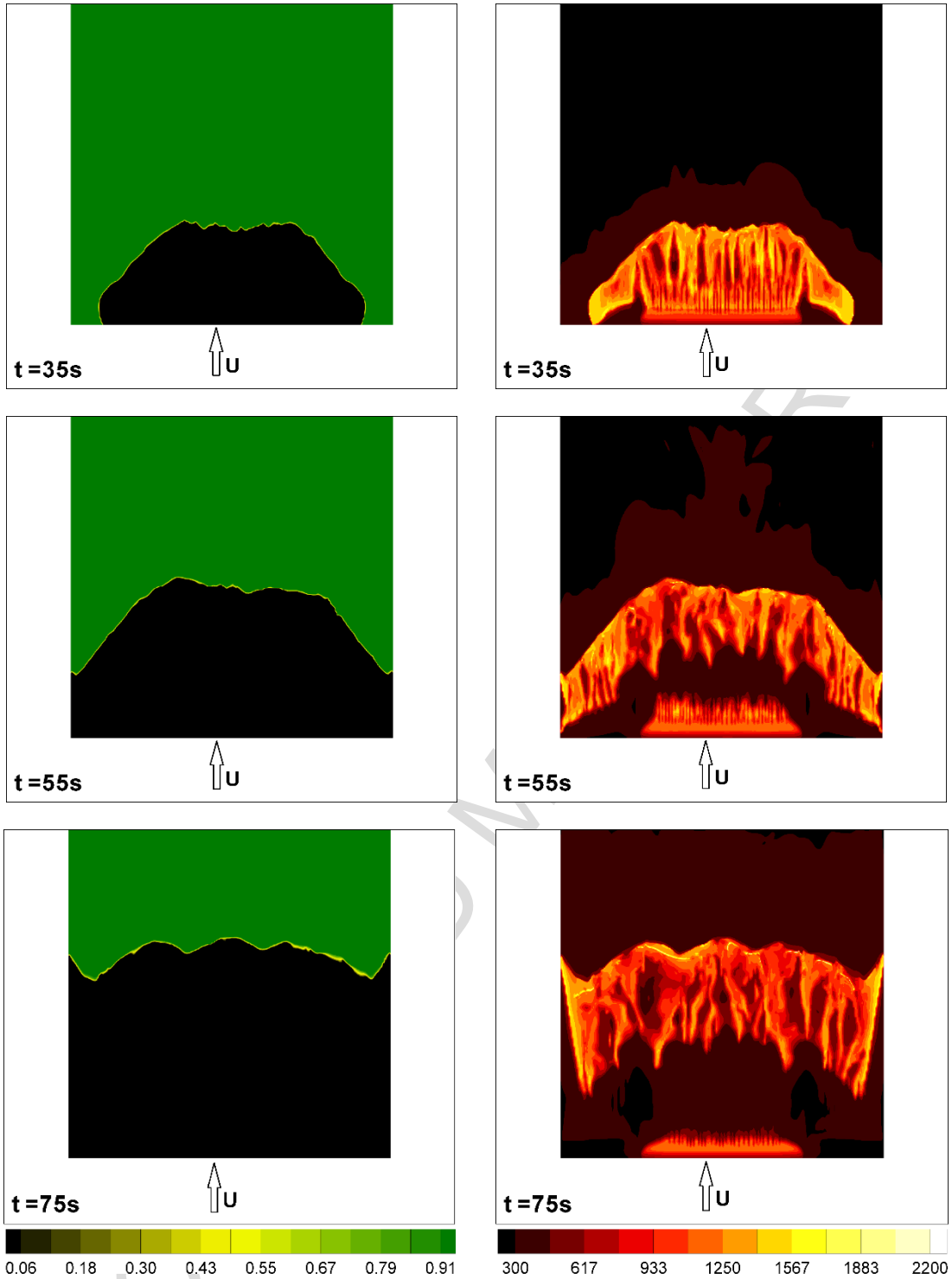


**Figure 4.** Top views of the computational domain (see Fig. 1) showing the propagation of a grassland fire in the case of a uniform fire-ignition mode (ignition at  $t = 10\text{ s}$ ), for a 10-m open wind speed  $U_{10} = 5\text{ m/s}$ . Left: mass fraction of dry material at vegetation height showing the shape of the pyrolysis front, right: temperature field (in Kelvin) at the surface of the solid fuel.

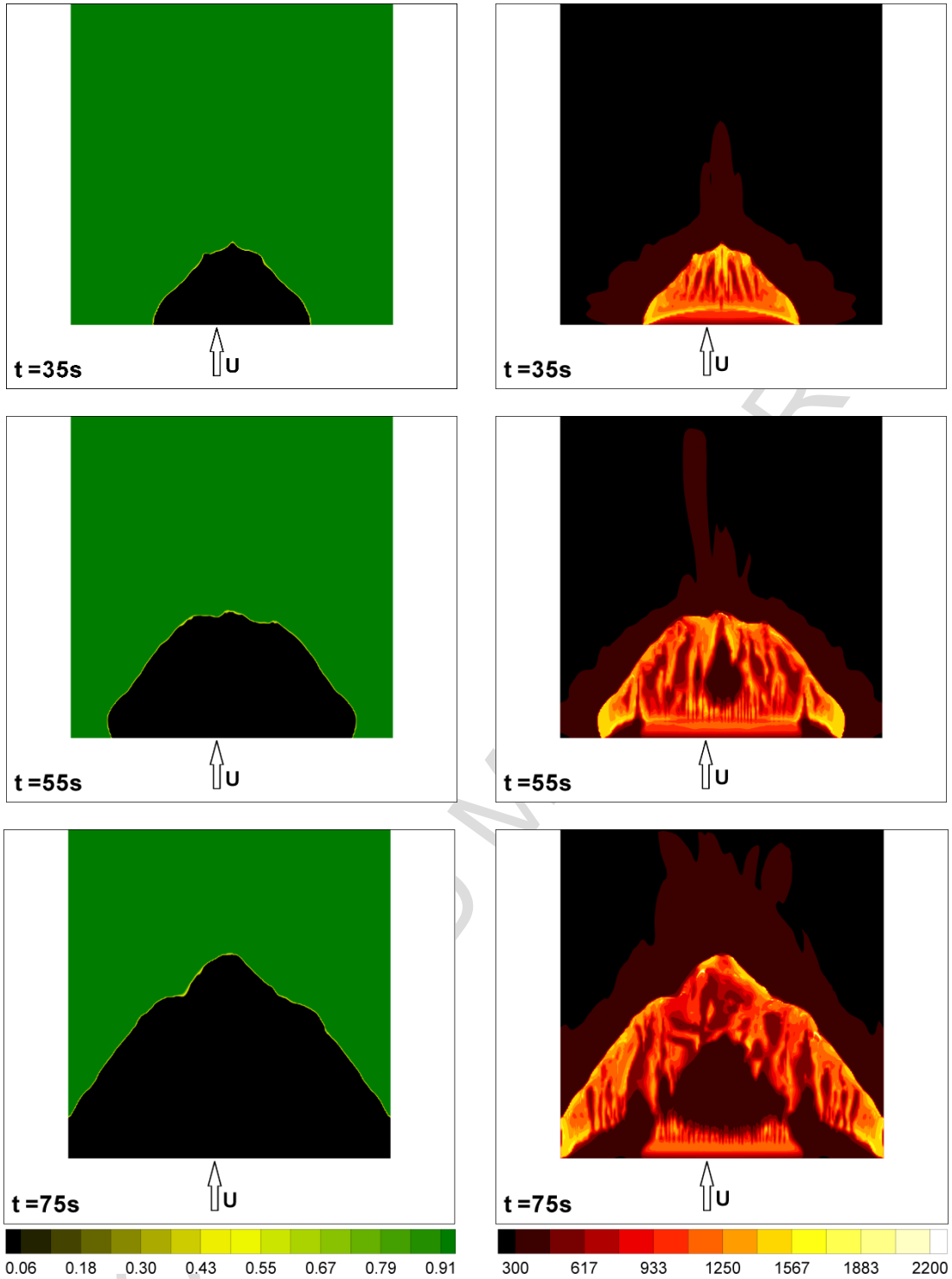


**Figure 5.** Top views of the computational domain (see Fig. 1) showing the propagation of a grassland fire in the case of a non-uniform fire-ignition mode (ignition at  $t = 10\text{ s}$ ), for a 10-m open wind speed  $U_{10} = 5\text{ m/s}$ . Left: mass fraction of dry material at vegetation height showing the shape of the pyrolysis front, right: temperature field (in Kelvin) at the surface of the solid fuel.

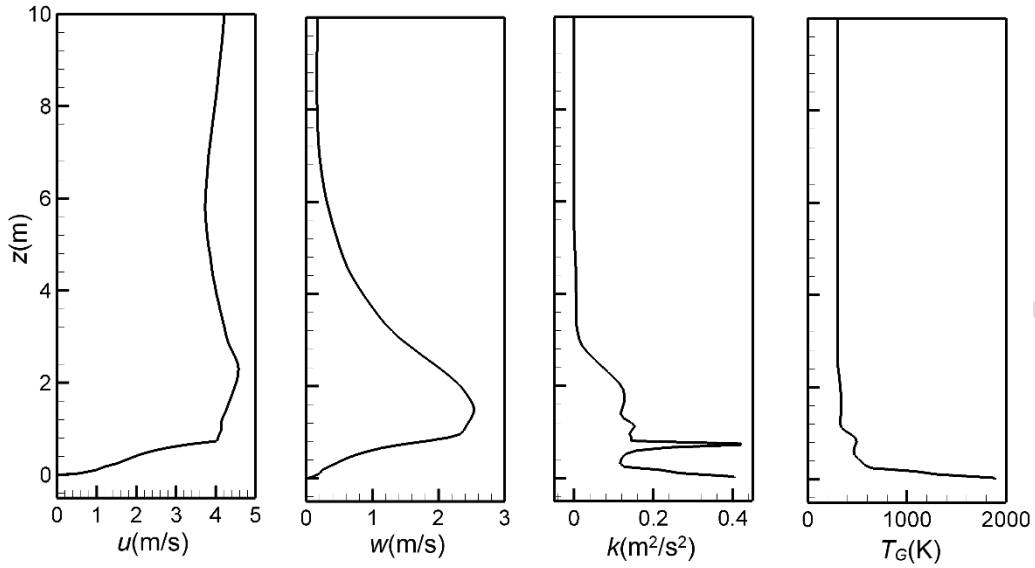


**Figure 6.** Vertical profiles of  $u$  and  $w$  ( $x$  and  $z$  components of the velocity),  $k$  (turbulent kinetic energy), and  $T_G$  (gas mixture temperature) obtained for  $U_{10} = 5$  m/s, in the case of a non-uniform fire-ignition, at  $t = 35$  s along line ( $y = 70$  m,  $x = 32.6$  m).

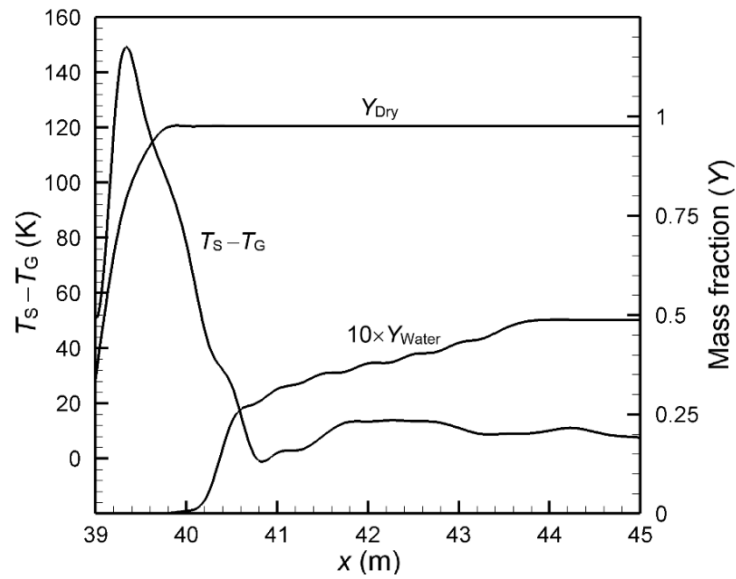


**Figure 7.** Temperature difference between the solid fuel and the gas mixture, dry material and water mass fractions along the line ( $y = 70$  m and  $z = \delta$ ) obtained at  $t = 35$  s, for a 10-m open wind speed  $U_{10} = 5$  m/s, in the case of a non-uniform fire-ignition mode.

3D views of the fire propagation obtained for a wind speed  $U_{10} = 5$  m/s and a non-uniform ignition mode are represented in Fig. 8. These figures are taken at two characteristic times before and when the fire front had reached the side limits of the plot. These results show clearly the potential of FireStar3D in reproducing numerically (at least qualitatively) the propagation of the fire through a grassland. The model is able to reproduce the characteristic parabolic shape of the fire front associated with this type of ignition procedure (see Fig. 3) as it was mentioned in experiments on the field [15,28].

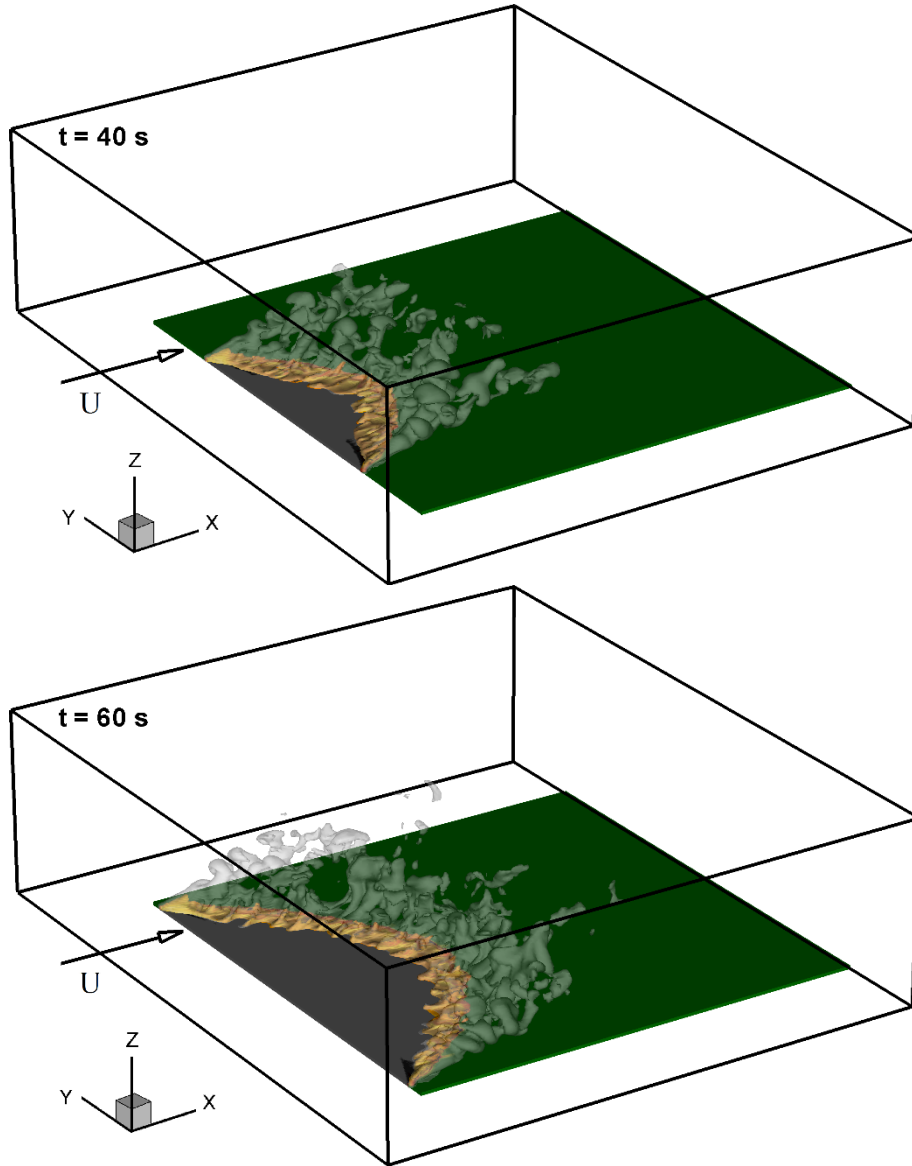


**Figure 8.** 3D View of one isovalue surface of the soot volume fraction ( $10^{-6}$ ) colored by the temperature of the gas (in yellow) and one isovalue surface of the water mass fraction ( $10^{-3}$ ) (in grey with 50% of transparency) for  $U_{10} = 5$  m/s and at different times, showing the fire propagation in the case of non-uniform fire-ignition mode.

To understand the effect of the wind speed on the flame structure and more generally on the dynamic of fire, 3D views of the fire propagation obtained for two extreme wind speed  $U_{10} = 1$  m/s and 10 m/s are shown in Fig. 9. It is obvious that for a small value of the wind speed ( $U_{10} = 1$  m/s), the flame plumes rise is not noticeably affected by the action of the cross wind. In this case the fire front can be assimilated to an obstacle, and the air flow is deflected vertically by the plume. On the other hand, Fig. 9 shows how larger value of wind speed ( $U_{10} = 10$  m/s) affects more significantly the rise of the flame plumes by crossing the fire front and pushing the hot gases toward the unburned vegetation. We can also notice that the wind speed increases significantly the depth of the fire front.



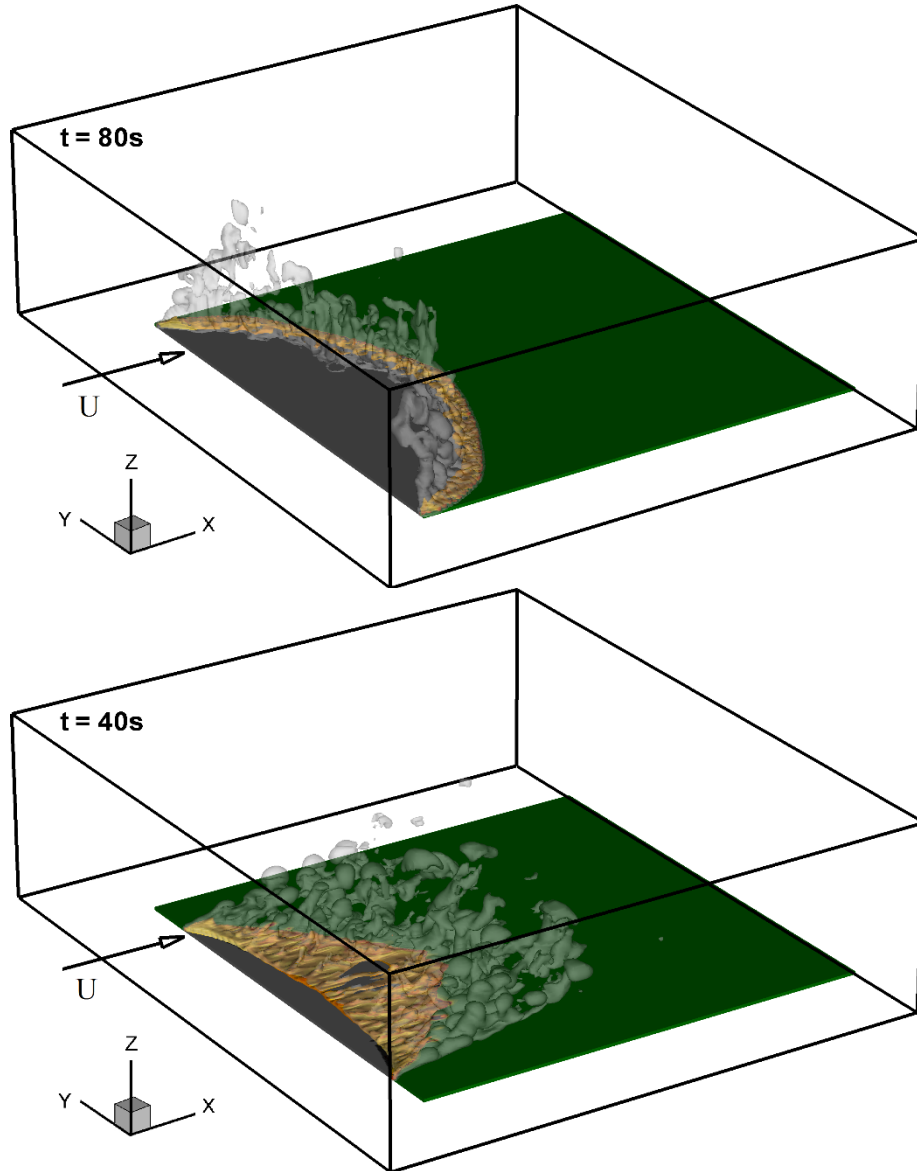


**Figure 9.** 3D View of one isovalue surface of the soot volume fraction ( $10^{-6}$ ) colored by the temperature of the gas (in yellow) and one isovalue surface of the water mass fraction ( $10^{-3}$ ) (in grey with 50% of transparency) for  $U_{10} = 1$  m/s (top) and  $U_{10} = 10$  m/s (bottom), showing the effect of wind speed on the fire dynamics in the case of non-uniform fire-ignition mode.

These phenomena are further illustrated by Fig. 10 showing cuts of the temperature and the flow fields (streamline) in the vertical median plane. For moderate wind conditions, we notice that the fresh air is sucked from the vicinity of the fire front supplying the thermal plume; the streamlines in Fig. 10 (top) show clearly the existence of aspiration regions ahead the fire front. In the literature, this regime is often referred to as “plume dominated fires”. As indicated previously, these results highlight the capability of the code to reproduce the backflow generated by the fire front on the leeward direction. In return for stronger wind conditions, the structure of the air flow is less affected by the fire front as shown in Fig. 10 (bottom), and this effect is limited to the local acceleration of the flow (resulting from a local expansion of the gas) in the plume and this regime is often referred to as “wind-driven fires”. The streamlines show clearly the possibility for



the inlet air flow to cross the fire front. For this interaction between the fire and the flow to be possible, the fire front must be structured vertically in peaks and troughs [54]. The reproduction of this configuration is not possible in 2D, because in 2D the fire front represents a uniform thermal barrier. This justifies the interest in analyzing the behavior of the fire using 3D simulations, even if much greater computational resources are required in this case. The interaction between the flames and the flow structures greatly affects heat transfer ahead of the fire front and, consequently fire propagation; this is clearly illustrated by Fig. 11. We notice that in the case of a “plume dominated fire” ( $U = 1$  m/s), radiative heat transfer prevails ahead of the fire front, indeed the temperature of the solid-fuel at the fuel-bed surface exceeds everywhere that of the gas mixture, and this temperature difference decreases uniformly with the distance from the flaming zone. In return, in the case of a “wind-driven fire” ( $U = 10$  m/s), the fluctuations of this temperature difference about zero is a clear signature of a prevailing convection heat transfer between the gas mixture and the fuel bed.

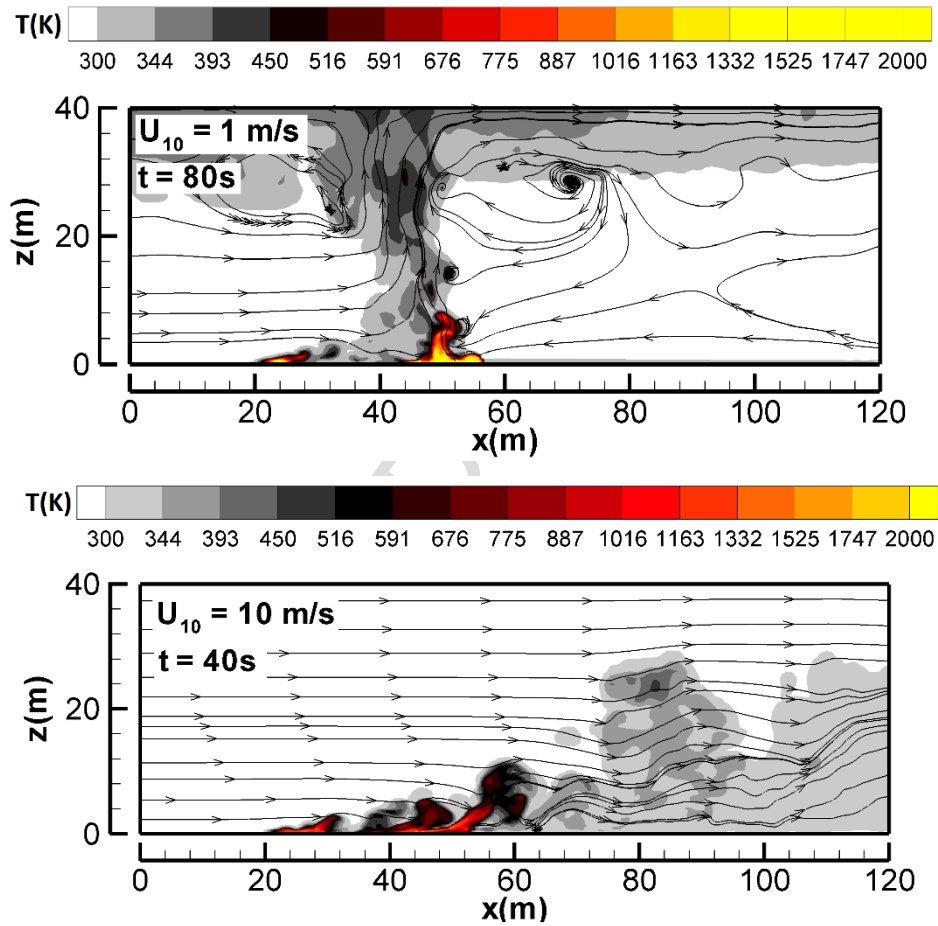


**Figure 10.** Temperature field and streamlines of the gaseous phase, obtained in the vertical median plane ( $y = 70$  m) for  $U_{10} = 1$  m/s (top) and  $U_{10} = 10$  m/s (bottom), showing the effect of wind speed on the fire dynamics in the case of non-uniform fire-ignition mode.

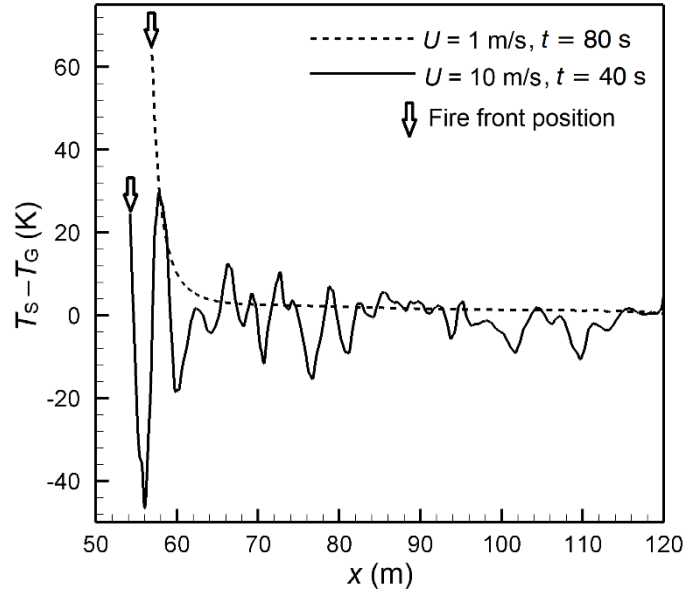


**Figure 11.** Temperature difference between the solid fuel and the gas mixture along the line ( $y = 70$  m and  $z = \delta$ ) ahead of the fire front, obtained in the case of a non-uniform fire-ignition mode for two different 10-m open wind speeds :  $U_{10} = 1$  m/s (at  $t = 80$  s) and  $U_{10} = 10$  m/s (at  $t = 40$  s), which corresponds to the temperature fields shown in Fig. 10.

To show the effect of wind speed on the flow structures, figure 12 shows, for two different wind speeds (1 and 10 m/s) and in the case of a non-uniform fire-ignition mode, isovalue surfaces of the  $Q$ -criterion colored by the vertical component of the velocity vector. This invariant of velocity gradient tensor represents the balance between the rotation and strain rates. The  $Q$ -criterion is an appropriate tool for the visualization of turbulent eddy formation, this criterion was introduced by Hunt et al. in 1988 [55]. The  $Q$  iso-surfaces are good indicators of coherent structures in a turbulent flow, this variable is defined as follows:

$$Q = \frac{1}{8} \left[ \left( \frac{\partial u_i}{\partial x_j} - \frac{\partial u_j}{\partial x_i} \right)^2 - \left( \frac{\partial u_i}{\partial x_j} + \frac{\partial u_j}{\partial x_i} \right)^2 \right] \quad (3)$$

where  $u_i$  is the velocity component in direction  $x_i$ . In addition of showing the three-dimensional nature of the flow, this figure highlights the flow structures present during a grassland fire. This figure clearly shows that the assumption of a homogeneous plane made for the fire front in the radiant panel theory is not valid, the fire front is structured as a succession of peaks and troughs allowing for the air flow to find a way across it [54]. This heterogeneity of the flame and the flow structure along the transverse direction, which is a great demonstration of 3D effects in a fire, affects a lot the propagation of the fire, as it has been clearly demonstrated experimentally at small scale [56] and numerically at larger scale [57]. The main effect is that, when the wind flow is able to cross the fire front, recirculating zones are formed at the back of the fire front, which redresses the flame and affects significantly the heat transfer between the flame and the vegetation and therefore the rate of spread. This effect is only visible above a certain threshold value of the wind speed. Being able to capture these flow details using an unsteady RANS approach is due to a relatively fine mesh resolution matching the extinction length scale ( $4/\alpha\sigma$ ) characterizing the absorption of the radiation inside the

vegetation layer. This leads us to possibly consider a fully Large Eddy Simulation (LES) approach using a comparable mesh resolution (that seems to be sufficient to capture the flow coherent structures), where a transport equation of the turbulent kinetic energy  $k$  only needs to be solved (instead of the two-equation  $k$ - $\varepsilon$  model).

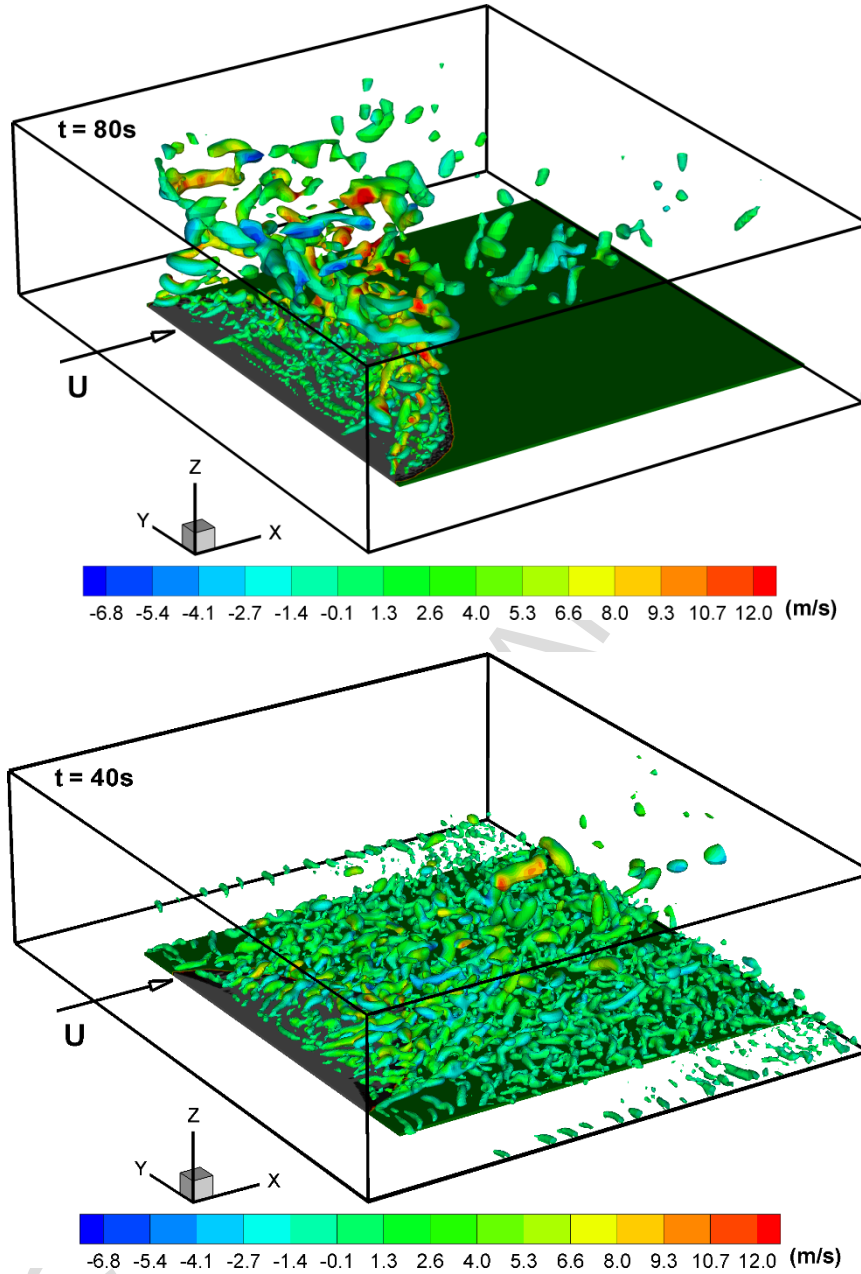


**Figure 12.** Flow structure in a grassland fire for two 10-m open wind speed  $U_{10} = 1$  m/s (top) and  $U_{10} = 10$  m/s (bottom) and for a non-uniform fire-ignition mode, shown using an isosurface of the  $Q$  criterion ( $Q = 0.5 \text{ s}^{-2}$ ) colored by the vertical component of the velocity field.

#### 4.2. Rate of Fire Spread

To go further in the analysis, we consider now two quantitative parameters, characterizing the fire: the Rate Of Spread (ROS) and the intensity of the fireline. The evolution of the ROS with the 10-m open wind speed ( $U_{10}$ ) is shown by Fig. 13. The ROS

estimation was obtained from the time derivative of the position of the pyrolysis front at the surface of the vegetation cover. Because this operation needs a certain level of regularity of the concerned curve, it was carried out in the vertical median plane (i.e. along the line  $y = 70 \text{ m}$ ,  $z = \delta$ ). Since the ignition procedure was initiated from the center to the sides, the head fire was always located in the median plane. Therefore this value can be considered to the same value of the rate of spread of the head fire, where the ROS reached its maximum value.

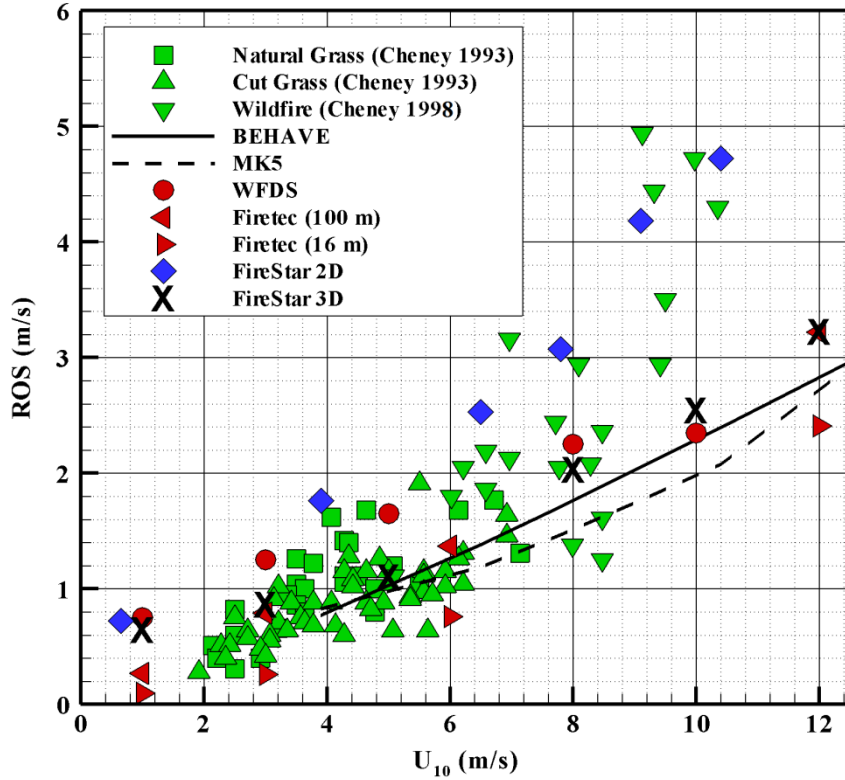


**Figure 13.** Rate of fire spread (ROS) through a uniform grassland obtained for different 10-m open wind speeds. The results of this study (FireStar3D) are compared to the results obtained experimentally (Cheney et al 1993, 1995, 1998 [27–29]), and using an empirical model (MK5 [8]), a semi-empirical model (BEHAVE [10]), 3D numerical models (FIRETEC [16], WFDS [15, 20]), and a 2D numerical model (FireStar2D [30]).

The experimental data shown in Fig. 13 were obtained from Cheney et al. [27–29] for different lengths  $w$  of the ignition line. These experimental studies show that the ROS increases with  $w$ , as found by FIRETEC model predictions (16 m and 100 m) [16], before reaching an asymptotic value for  $w > 200 \text{ m}$ . For example, when  $w$  increased from 50 m to 250 m, the ROS increased by about 30% for  $U_{10} = 3 \text{ m/s}$  and  $6 \text{ m/s}$ . The authors reported that this scale effect was more pronounced for larger wind speeds. Concerning the relatively large dispersion of the experimental measurements, it can result from the unsteadiness nature of the wind flow [58]. On the other hand, the reported experimental data for  $U_{10} \geq 8 \text{ m/s}$  [29] were estimated from measurements recorded during real wildfires with significantly large fire front (the ROS reaches its maximum value) but for which wind speed and vegetation characteristics are not under control as in experimental fires. We recall that the simulations were carried out under conditions similar to those of experiment C064 conducted by Cheney et al. [28]. The main difference lies in the grass height ( $\delta = 0.7 \text{ m}$  in the simulations compared to  $\delta = 0.21 \text{ m}$  for experiment C064) and

this choice was mainly motivated by the existence of prior numerical studies [16,30]. For low to moderate  $U_{10}$  values (up to 6 m/s), FireStar3D results compare well with experimental data and with other predictions, and we can observe a quasi-linear evolution of the ROS. Between 1 and 5 m/s we can notice a less influence of the wind speed upon the rate of spread, this result is compatible with the transition between a plume dominated fire (for  $U_{10} = 1$  m/s) and a wind driven fire ( $U_{10} = 5$  m/s)[58,59]. For these values of wind speed, a steady regime of fire propagation was clearly reached in the simulations, as shown by Fig. 14 for  $U_{10} = 1$  m/s from the regular and constant slope of the fire front position versus time. For  $U_{10} = 8$  m/s, the results are consistent with the predictions of other models and with the experiments, despite the relative dispersion of the experimental measurements which prevents a significant comparison. For  $U_{10} \geq 10$  m/s, FireStar3D clearly underestimates the ROS (just as FIRETEC and WFDS do) mainly because of the short ignition-line length of 50 m that has been considered and also because of the longitudinal extension of the plot (100 m) which were too short to reach quasi-steady conditions of propagation, as shown by Fig. 14 for  $U_{10} = 10$  m/s from the highly irregular evolution of the fire front position with time.

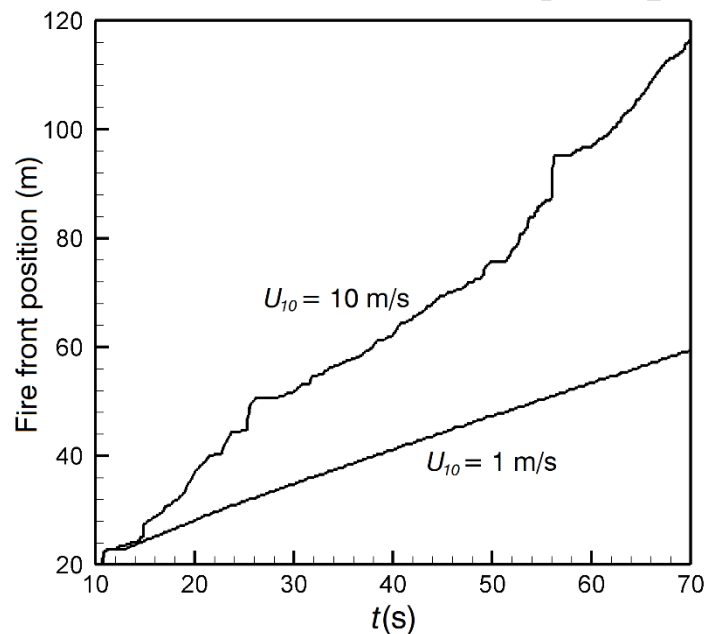


**Figure 14.** Position versus time of the furthestmost point of the pyrolysis front at the fuel-bed surface obtained in the case of a non-uniform fire-ignition mode for two different 10-m open wind speeds :  $U_{10} = 1$  m/s and  $U_{10} = 10$  m/s.

To illustrate further this last point, the results obtained with WFDS reported in Fig. 13, were obtained with a plot 50 m long, with a consequence that the ROS seems to saturate above a certain value of the wind speed (8 m/s). On the other hand, FireStar2D that assumes a straight and infinite pyrolysis front better predicts the ROS at high wind speeds (10 m/s and 12 m/s). In return, 2D models fail to account for the aerodynamic drag on the lateral border of the fire front that is primarily responsible for its curvature, which results in the overestimation of the ROS at low to moderate wind speeds. Both for the empirical model (MK5) and semi-empirical one (BEHAVE), the experimental fires that helped elaborating them could not be carried out properly for wind speeds exceeding the threshold value of 7-8 m/s [10], leading to an underestimation of the ROS by these models at high wind speeds. We can explain the discrepancies between MK5, BEHAVE and field

measurements by the fact that for safety reasons the experiments carried out to elaborate the MK5 model cannot be conducted under strong wind conditions, whereas for BEHAVE model there is a real scaling problem in extrapolating experimental data collected at small scale in a wind-tunnel to fires at large scale such as in grassland.

### 4.3. Fire Intensity

The fireline intensity ( $I_{BYR}$ ) at the center of the fire front (maximum value) can be evaluated from Eq. 4 (Byram's intensity [60]), where  $m = \alpha\rho\delta$  is the fuel load (equal to 0.7 kg/m<sup>2</sup> according to Tab. 1), and  $\Delta H$  is the heat yield of the fuel (estimated at about 18000 kJ/kg [61]).

$$I_{BYR} = m \times \Delta H \times ROS \quad (4)$$

Because this approximation is theoretically valid only for a straight front propagating at the same speed, we have chosen to evaluate numerically the fireline intensity from the Heat Release Rate (HRR) defined by Eq. 5 as the product of  $\Delta H$  and the rate of total mass-loss of vegetation in the entire computational domain.

$$I = \dot{m} \times \Delta H \quad (5)$$

The time evolution of the heat release rate, evaluated from Eq. 5 with  $\Delta H = 18\,000$  kJ/kg, are shown in Fig. 15 (for three values of wind speed). The figure shows that the heat release rate grows until the lateral branch of the fire reach the limit of the plot, more or less at the same time (75 s) for these three values of the wind speed, mainly because the propagation of the flank fire is less affected by the air flow.

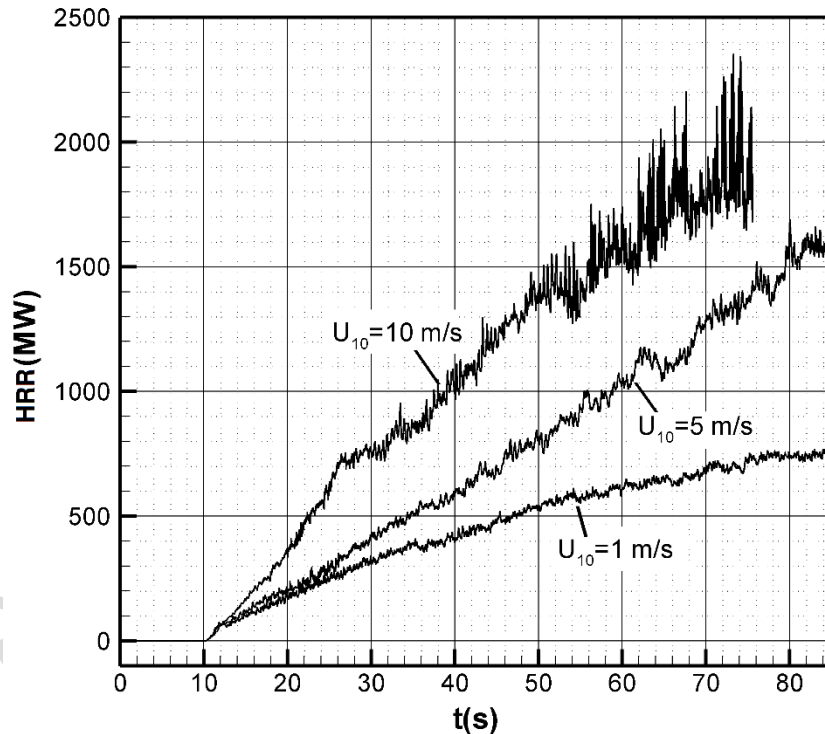


**Figure 15.** Time evolution of the Heat Release Rate (HRR) of the fire obtained from the rate of total mass-loss evaluated for the whole solid-fuel layer, in the case of non-uniform fire-ignition mode, for three different 10-m open wind speed  $U_{10} = 1, 5$ , and 10 m/s. For  $U_{10} = 10$  m/s, the fire front reaches the end of the domain around  $t = 76$  s.



The fireline intensity can be estimated numerically by dividing the average value of the heat release rate reached when the fire was fully developed ( $HRR_{\infty}$ ) by the width  $w$  of the plot (100 m) according to Eq. 6.

$$I \approx \frac{HRR_{\infty}}{w} \quad (6)$$

Using the fire line intensity calculated from Eq. 6, it is then possible to evaluate Byram's convective number  $N_c$  defined as the ratio between the buoyancy force and the inertial force due to the wind [59] and given by Eq. 7, where  $g$  is the acceleration of gravity (9.81 m/s<sup>2</sup>), and  $\rho_0$  (1.171 kg/m<sup>3</sup>) and  $C_{p0}$  (1010 J/kg.K) are the density and the specific heat of ambient air at temperature  $T_0 = 300$  K.

$$N_c = \frac{2 g I}{\rho_0 C_{p0} T_0 (U_{10} - ROS)^3} \quad (7)$$

Byram's convective number is an indicator of the fire propagation regime. Large values of Byram's number are normally obtained in fires governed by plumes (plume dominated fires), with a heat transfer between the flame and the vegetation dominated by radiation. Whereas small values of Byram's number are obtained in fires piloted by inertial effects (wind driven fire), with a more important contribution of the convection heat transfer [14,59].

A comparison between the two methods of calculation of the fireline intensity ( $I_{BYR}$  obtained from Eq. 4 and  $I$  obtained successively from Eqs. 5 and 6) is presented in Tab. 2. We can notice that the deviation between these two approaches increases with the wind speed: for  $U_{10} = 1$  m/s, the relative variation  $\Delta I/I$  is equal to 26%, while for  $U_{10} = 12$  m/s,  $\Delta I/I$  is equal to 101%. Two factors can explain these differences: (1) in the calculation of  $I_{BYR}$  the rate of spread was evaluated at the center of the front line (where the ROS was maximum) and averaged over the propagation time of the fire; and (2) it was assumed that all the solid fuel had burned. Both these effects result in an overestimation of the quantity of fuel consumed by the fire and are therefore responsible for the overestimation of  $I_{BYR}$  (as seen in Tab. 2). Furthermore, these effects become more pronounced as the wind speed increases, which explains why the relative difference  $\Delta I/I$  was smaller for a wind speed of 1 m/s than for 12 m/s.

$U_{10}$ (m/s)	1	3	5	8	10	12
$I_{BYR}$ (kW/m)	8820	11340	15120	25200	31500	40320
$I$ (kW/m)	7000	8000	14000	17000	19000	20000

**Table 2.** Fireline intensity evaluated using two approaches: (1) from the average rate of spread and assuming that the initial fuel load had fully burned ( $I_{BYR}$ , Eq. 4) and (2) from the rate of total mass-loss of solid fuel ( $I$ , Eq. 6).

To illustrate the relation between Byram's convection number and the fire regime, we notice for example that for a 10-m open wind speed  $U_{10} = 1$  m/s, Byram's number  $N_c$ , estimated from Eq. 7 using the value of the ROS from Fig. 14 and the value of  $I$  from Tab. 2, is about 14300, while for  $U_{10} = 10$  m/s,  $N_c$  is about 2.5. We can conclude that the situation observed for  $U_{10} = 1$  m/s was clearly a plume dominated fire, and that for  $U_{10} =$

10 m/s the situation was closer to a wind driven fire. The ratio  $ROS/U_{10}$  versus the inverse of Byram's convective number  $N_c$  (calculated from Eq. 7) is shown in Fig. 16, where the numerical results are compared to experimental data collected from the various experimental campaigns carried out in Australia [27–29, 62]. Despite some discrepancies between numerical and experimental data, the two sets of data compare relatively well. As pointed out in a previous study [17,58], the maximum value of the ratio  $ROS/U_{10}$  (equal to 0.7 in our case) is obtained for fires dominated by buoyancy (plume dominated fires), and thus for small values of the ratio  $1/N_c$ . On the other side of the curve (i.e. for large values of  $1/N_c$ ), the ratio  $ROS/U_{10}$  tends towards a constant value (nearly equal to 0.25). That means that for fires dominated by inertial forces (wind driven fires) the ROS converges toward a linear relationship with the wind speed. This behavior has been reported by many experimental studies, in various ecosystems (surface fires in grassland, shrubland ...) [62]. The relatively high values observed for the two branches of the curve (comparable to the values observed on the field), can be interpreted as a consequence of the low value of the fuel moisture content ( $M = 5\%$ ) that contributes significantly to promote the propagation of the fire, and therefore to obtain high rates of spread.

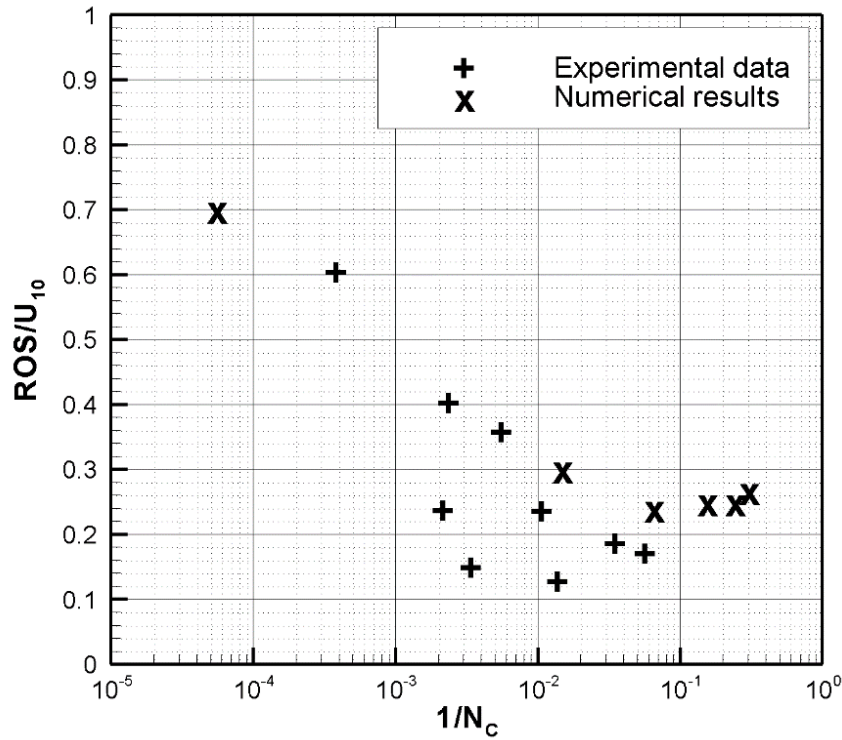


**Figure 16.** Ratio  $ROS/U_{10}$  versus the inverse of Byram's convective number  $N_c$ , comparison between numerical results and experimental data [62].

## 5. Conclusions

This study reported numerical simulations of fire spread through a homogeneous grassland. The results were obtained using a 3D Computational Fluid Dynamic code based on a fully-physical multiphase model. At low to moderate wind speeds (up to 8 m/s), the simulated Rate Of Spread of fire (ROS) was in good agreement with the data of the experimental campaign conducted in Australia, with the predictions of operational empirical models (such as MK5 and BEHAVE), and with



the numerical results of other 3D physical models (FIRETEC and WFDS). At high wind speeds (10 m/s and 12 m/s), a larger extends of the vegetation cover and a larger length of the ignition-line would be required in order to reach the asymptotic values of the ROS. Nevertheless, the results of FireStar3D were in good agreement with the predictions of other 3D physical models (FIRETEC and WFDS). The study has also shown that the method of fire ignition can affect significantly the shape of the fire front without affecting significantly the rate of fire spread. Consequently, it seems that the non-uniform fire-ignition of the grassland (consistent with the experimental procedure) allows recovering the parabolic shape of the fire front observed experimentally. The analysis of the results by exploiting the rate of total mass-loss of solid fuel has allowed to reconstruct the evolution of the ratio  $ROS/U_{10}$  as a function of the inverse of Byram's convective number. This parameter is a good indicator to highlight the existence of two propagation regimes of surface fires, namely the plume dominated and the wind driven fires. The next step of this work, would be to explore the 3D interactions between a quasi-infinite width fireline (reproduced using periodic conditions at the lateral boundaries of the fuel layer) and the atmospheric boundary layer. Various aspects of this problem could be studied, such as the impact of the unsteady nature of the wind speed, the competition between the inertial forces and buoyancy, the aerology generates by the fire itself, the coherent structures observed along the fire front and their impact upon the fire dynamic. These aspects would be better addressed using the new simplified LES model implemented in FireStar3D. This model had been validated in the case of an isothermal flow through homogenous and inhomogeneous canopies [25, 26], and has been recently extended to account for fire propagation. Many other fundamental aspects of the wildfire dynamic are not well understood, such as the role played by the field slope (and the competition between the wind and the slope when their directions are not aligned), the impact of the fuel moisture content (its threshold effect in the burn/no burn process, the linear or exponential decay of the rate of spread ...). In complement to experimental investigations, detailed physical models (such as Firestar3D) could be good tools for the understanding of the basic physical processes governing the behavior of wildfires. In more practical contexts, this kind of numerical simulation tools can be used to analyze the effects of the vegetation layer properties (heterogeneity, discontinuity ...) or to simulate some operational situations, such as prescribed burning (to evaluate the thermal impact in the soil), counter-fires ignited during firefighting operations [20], or to study the efficiency of a fuel break [19].

## Acknowledgements

This work was granted access to the HPC resources of Aix-Marseille Université funded by the project Equip@Meso (ANR-10-EQPX-29-01) of the program "Investissements d'Avenir" supervised by the "Agence Nationale pour la Recherche". The authors thank the anonymous reviewers for the quality of their analysis, their reports have contributed a lot to improve the paper.

## References

- [1] R.J. Whelan, The ecology of fire, Cambridge studies in ecology, 1st Edition, 1995.
- [2] S.J. Pyne, P.L. Andrews, R.D. Laven, Introduction To Wildland Fire, John Wiley & Sons, New York, 2nd Edition, 1996.
- [3] W.T. Sommers, S.G. Coloff, S.G. Conard, Synthesis of Knowledge: Fire History and Climate Change, JFSP Synth. Reports. Pap. 19. (2011) 190.
- [4] M.G. Cruz, A.L. Sullivan, J.S. Gould, N.C. Sims, A.J. Bannister, J.J. Hollis, R.J. Hurley, Anatomy of a catastrophic wildfire: The Black Saturday Kilmore East fire in Victoria, Australia, For. Ecol. Manage. 284 (2012) 269–285.
- [5] Parliament of Victoria, 2009 Victorian Bushfires Royal Commission, in: 2009 Vic. Bushfires R. Comm., 2010.
- [6] K.G. Tolhurst, B. Shields, D.M. Chong, Phoenix: Development and Application of a Bushfire Risk Management Tool, Aust. J. Emerg. Manag. 23 (2008) 47.
- [7] M.A. Finney, FIRESITE: Fire Area Simulator-Model Development and Evaluation, RMRS-RP-4, Ogden, UT. (1998) 47.
- [8] A.G. McArthur, Weather and Grassland Fire Behaviour, Leaflet No. 100, Canberra Aust. For. Timber Bur. (1966) 23.
- [9] A.G. McArthur, Fire behaviour in eucalypt forests, Leaflet No. 107, For. Res. Institute, Canberra, Aust. (1967).
- [10] R.C. Rothermel, A mathematical model for predicting fire spread in wildland fuels, USDA For. Serv. Res. Pap. INT USA. (1972) 40.
- [11] H.P. Hanson, M.M. Bradley, J.E. Bossert, R.R. Linn, L.W. Younker, The potential and promise of physics-based wildfire simulation, Environ. Sci. Policy. 3 (2000) 161–172.
- [12] A.L. Sullivan, Wildland surface fire spread modelling, 1990–2007. 1: Physical and quasi-physical models, Int. J. Wildl. Fire. 18 (2009) 349–368.
- [13] A.M. Grishin, Mathematical modeling of forest fires and new methods of fighting them, edited by F. A. Albin, Publishing House of the Tomsk University, Tomsk, Russia, in: 1997.
- [14] D. Morvan, Physical Phenomena and Length Scales Governing the Behaviour of Wildfires: A Case for Physical Modelling, Fire Technol. 47 (2011) 437–460.
- [15] W. Mell, M.A. Jenkins, J. Gould, P. Cheney, A physics-based approach to modelling grassland fires, Int. J. Wildl. Fire. 16 (2007) 1–22.
- [16] R.R. Linn, P. Cunningham, Numerical simulations of grass fires using a coupled atmosphere-fire model: Basic fire behavior and dependence on wind speed, J. Geophys. Res. 110 (2005) D13107.
- [17] D. Morvan, S. Meradji, G. Accary, Wildfire behavior study in a mediterranean pine stand using a physically based model, Combust. Sci. Technol. 180 (2008) 230–248.
- [18] D. Morvan, J.L. Dupuy, Modeling the propagation of a wildfire through a Mediterranean shrub using a multiphase formulation, Combust. Flame. 138 (2004) 199–210.
- [19] D. Morvan, Numerical study of the behaviour of a surface fire propagating through a firebreak built in a Mediterranean shrub layer, Fire Saf. J. 71 (2015) 34–48.
- [20] D. Morvan, S. Meradji, W. Mell, Interaction between head fire and backfire in grasslands, Fire Saf. J. 58 (2013) 195–203.
- [21] W. Mell, S. Manzello, A. Maranghides, The Wildland-Urban Interface Problem - Current Approaches and Research Needs, Int. J. Wildl. Fire. 19 (2010) 238.
- [22] E. Koo, R.R. Linn, P.J. Pagni, C.B. Edminster, Modelling firebrand transport in wildfires using HIGRAD/FIRETEC, Int. J. Wildl. Fire. 21 (2012) 396–417.
- [23] G. Accary, S. Meradji, D. Morvan, D. Fougère, FireStar3D-3D finite volume model for

- the prediction of wildfires behavior. *Advances in Forest Fire Research*, in: D.X. Vegas Editor, (2014) 251–261.
- [24] G. Accary, S. Meradji, D. Morvan, D. Fougère, Towards a numerical benchmark for 3D mixed-convection low Mach number flows in a rectangular channel heated from below, *Fluid Dyn. Mater. Process.* 141 (2008) 1–7.
- [25] K. Gavrilov, G. Accary, D. Morvan, D. Lyubimov, S. Méradji, O. Bessonov, Numerical simulation of coherent structures over plant canopy, *Flow, Turbul. Combust.* 86 (2011) 89–111.
- [26] K. Gavrilov, D. Morvan, G. Accary, D. Lyubimov, S. Meradji, Numerical simulation of coherent turbulent structures and of passive scalar dispersion in a canopy sub-layer, *Comput. Fluids.* 78 (2013) 54–62.
- [27] N.P. Cheney, J.S. Gould, W.R. Catchpole, The influence of fuel, weather and fire shape variables on fire spread in grasslands, *Int. J. Wildl. Fire.* 3 (1993) 31–44.
- [28] N.P. Cheney, J.S. Gould, Fire growth in grassland fuels, *Int. J. Wildl. Fire.* 5 (1995) 237–247.
- [29] N.P. Cheney, J.S. Gould, W.R. Catchpole, Prediction of fire spread in grasslands, *Int. J. Wildl. Fire.* 8 (1998) 1–13.
- [30] D. Morvan, S. Méradji, G. Accary, Physical modelling of fire spread in Grasslands, *Fire Saf. J.* 44 (2009) 50–61.
- [31] A. Favre, L.S.G. Kovasznay, R. Dumas, J. Gaviglio, M. Coantic, *La turbulence en mécanique des fluides*. Gauthier-Villars, 1976.
- [32] G. Cox, *Combustion fundamentals of fire*. Academic Press, (1995).
- [33] V. Yakhot, L.M. Smith, The renormalization group, the epsilon-expansion and derivation of turbulence models, *J. Sci. Comput.* 7 (1992) 35–61.
- [34] S.A. Orszag, I. Staroselsky, W.S. Flannery, Y. Zhang, *Introduction to renormalization group modeling of turbulence*. Oxford University Press, Simul. Model. Turbul. Flows. (1996) 155–183.
- [35] R.J. Kee, F.M. Rupley, J.A. Miller, *The Chemkin Thermodynamic Data Based*, Sandia Natl. Lab. (1992).
- [36] B.F. Magnussen, B.H. Mjertager, On mathematical modeling of turbulent combustion, *Combust. Sci. Technol.* 140 (1998) 93–122.
- [37] K.J. Syed, C.D. Stewart, J.B. Moss, Modelling soot formation and thermal radiation in buoyant turbulent diffusion flames. In 23rd Symposium (International) on combustion, The Combustion Institute, Pittsburgh, 23 (1991) 1533–1541.
- [38] J.B. Moss, *Turbulent Diffusion Flames*. In G. Cox (Ed.), Academic Press, London, UK, 1990.
- [39] J. Nagle, R.F. Strickland-Constable, Oxidation of Carbon Between 1000–2000°C, *Proc. Fifth Conf. Carbon.* (1962) 154–164.
- [40] F.P. Incropera, D.P. DeWitt, *Fundamentals of Heat and Mass Transfer*, John Wiley and Sons, 1996.
- [41] R. Siegel, J.R. Howell, *Thermal Radiation Heat Transfer*. Hemisphere Publishing Corporation, Washington D.C., 3rd edition, 1992.
- [42] S. V. Patankar, *Numerical Heat Transfer and Fluid Flow*. Hemisphere Publishing, New York, 1980.
- [43] Y. Li, M. Rudman, Assessment of higher-order upwind schemes incorporating FCT for convection-dominated problems, *Numer. Heat Transf. Part B Fundam.* 27 (1995) 1–21.
- [44] H.K. and M. Versteeg W, *An introduction to Computational Fluid Dynamics, The Finite Volume Method*. Prentice Hall, (2007).

- [45] J.H. Ferziger, M. Peric, A. Leonard, Computational Methods for Fluid Dynamics. Springer-Verlag, (2002).
- [46] M.F. Modest, Radiative Heat Transfer Academic Press, (2003).
- [47] C.R. Kaplan, S.W. Bek, E.S. Oran, Ellzey J L, Dynamics of a Strongly Radiating Insteady Ethylene Jet Diffusion Flame, Combust. Flame. 96 (1994) 1–21.
- [48] G. Accary, O. Bessonov, D. Foug, Optimized Parallel Approach for 3D Modelling of Forest Fire Behaviour, V.E. Malyshkin (Ed.), PaCT 2007, LNCS, Springer, Heidelb. 4671 (2007) 96–102.
- [49] G. Accary, O. Bessonov, D. Foug, Efficient Parallelization of the Preconditioned Conjugate Gradient Method, V.E. Malyshkin (Ed.), PaCT 2009, LNCS, Springer, Heidelb. 5968 (2009) 60–72.
- [50] A. Khalifeh, G. Accary, S. Meradji, G. Scarella, D. Morvan, K. Kahine, Three-dimensional numerical simulation of the interaction between natural convection and radiation in a differentially heated cavity in the low Mach number approximation using the discrete ordinates method, in: Proc. Fourth Int. Conf. Therm. Eng. Theory Appl. Abu Dhabi, UAE, 2009.
- [51] A.G. McArthur, Grassland Fire Danger Meter MkV. CSIRO Division of Forest. Annual Report, 1977.
- [52] R.E. Burgan, R.C. Rothermel, Behave: Fire Behavior Prediction and Fuel Modeling System - FUEL Subsystem, Behave. Intermount (1984).
- [53] W. Mell, J. Charney, M. Jenkins, Numerical simulations of grassland fire behavior from the LANL-FIRETEC and NIST-WFDS models. George Mason University, Fairfax, VA, in: EastFIRE Conf., 2005: pp. 1–10.
- [54] T. Beer, The interaction of wind and fire, Boundary-Layer Meteorol. 54 (1991) 287–308.
- [55] J.C.R. Hunt, A.A. Wray, P. Moin, Eddies, streams, and convergence zones in turbulent flows, Stud. Turbul. Using Numer. Simul. Databases, 2. Proc. 1988 Summer Progr. 1 (1988) 193–208.
- [56] M.A. Finney, J.D. Cohen, J.M. Forthofer, S.S. McAllister, M.J. Gollner, D.J. Gorham, K. Saito, N.K. Akafuah, B.A. Adam, J.D. English, Role of buoyant flame dynamics in wildfire spread, in: Proc. Natl. Acad. Sci., 2015: pp. 9833–9838.
- [57] R.R. Linn, J.M. Canfield, P. Cunningham, C. Edminster, J.L. Dupuy, F. Pimont, Using periodic line fires to gain a new perspective on multi-dimensional aspects of forward fire spread, Agric. For. Meteorol. 157 (2012) 60–76.
- [58] D. Morvan, Wind effects, unsteady behaviors, and regimes of propagation of surface fires in open field, Combust. Sci. Technol. 186 (2014) 869–888.
- [59] R.M. Nelson, Re-analysis of wind and slope effects on flame characteristics of Mediterranean shrub fires, Int. J. Wildl. Fire. 24 (2015) 1001–1007.
- [60] G.M. Byram, Forest Fire Control and Use in K.P. Davis (Ed.), McGraw-Hill, New York., 1959.
- [61] P. Cheney, A. Sullivan, Grassfires : Fuel, Weather and Fire Behaviour, Behaviour. (2008) 0–16.
- [62] A.L. Sullivan, Convective Froude number and Byram's energy criterion of Australian experimental grassland fires, Proc. Combust. Inst. 31 II (2007) 2557–2564.

- Numerical simulations of grassland fire
- Detailed physical fire model
- Plume dominated fire, wind driven fire
- Byram's convective number